3d spectator hole satellites of the Cu $K\beta_{1,3}$ and $K\beta_{2,5}$ emission spectrum

H. Enkisch, C. Sternemann, M. Paulus, M. Volmer, and W. Schülke

Institute of Physics, University of Dortmund, D-44221 Dortmund, Germany

(Received 8 December 2003; published 19 August 2004)

The intensity evolution of the Cu $K\beta_{1,3}$ and $K\beta_{2,5}$ emission spectra is measured as a function of excitation energy using resonant inelastic x-ray scattering spectroscopy. The contribution of $\underline{1s3d}$ shake satellites to the Cu $K\beta_{1,3}$ as well as to the Cu $K\beta_{2,5}$ emission spectrum is extracted. Both emission spectra indicate an additional contribution of $\underline{1s3p}$ shake satellites. The intensity evolution of the shake satellites from threshold to saturation is compared to the Thomas model and shows a similar saturation behavior as found for the Cu $K\alpha_{1,2}$ $\underline{1s3d}$ shake satellites, stating that the shake process is independent of the reemission shell. These $\underline{1s3d}$ shake satellites rapidly reach their saturation limit in contrast to Cu $\underline{1s2p}$ and $\underline{1s1s}$ shake satellites. Furthermore, the contribution of the *KMN* and the *KNN* radiative Auger satellites to the Cu $K\beta_{1,3}$ and Cu $K\beta_{2,5}$ emission spectra is obtained, respectively. The *KNN* radiative Auger satellite is shown to play an important role in the interpretation of valence fluorescence spectra.

I. INTRODUCTION

Multielectron excitations during inner-shell vacancy creation due to atomic inner-shell electron correlations have been extensively studied in the so-called isothermal regime high above the double-excitation thresholds [1] and recently also in the adiabatic regime close to the excitation threshold [2]. In the isothermal regime the excitation processes can be treated to be independent. This is not valid in the adiabatic limit where the inner-shell vacancy creation along with the excitation of a second electron has to be treated as a single process. The ejection of a second electron during ionization and inner-shell excitation can occur to unoccupied bound states (shake-up) as well as to continuum states (shake-off) [3,4] and causes discontinuities in x-ray absorption [5–10] and additional structures in photoemission and inverse photoemission spectra [2,11–13].

With the advent of third-generation synchrotron sources the measurement of x-ray fluorescence emission spectra became more prominent as an alternative method to study multielectron excitations [14,15]. It has been successfully applied to a wide range of materials—e.g., Cu [16–19], Ge [20], W [21], Ar [22], and most recently to NaF [23]. In this spectroscopy the multielectron processes described above exhibit a strong change of fluorescence line shape due to so-called satellite or spectator-hole lines. Beyond this, the shape of the fluorescence lines can be strongly affected also by the resonant Raman effect [24,25] and radiative Auger satellites (RAS's) [26–29].

Cu is indisputably the best studied material with respect to multielectron effects utilizing x-ray fluorescence spectroscopy. Deutsch *et al.* [15] measured the Cu $K\alpha_{1,2}$ and Cu $K\beta_{1,3}$ x-ray emission spectra in the isothermal regime. They compared the spectra with fits to realtivistic Dirac-Fock calculations of the possible transitions and found a 26–30% contribution of $\underline{1s3d}$ spectator transitions to the total emission spectrum while the contributions from $\underline{1s3s}$ and $\underline{1s3p}$ transitions were negligible.

The intensity evolution from the adiabatic to the isothermal regime was measured first for the Cu $\underline{1s2p}$ satellite spec-

trum of the Cu $K\alpha_{1,2}$ emission [16,17] followed by a study of the Cu $\underline{1s1s}$ hypersatellites [18]. These satellite spectra when related to deep-core electron shake excitation show clear shake-off behavior with respect to their intensity evolution. For both satellites the fit to the Thomas model [30], which describes the intensity evolution of the double-excitation processes within time-dependent perturbation theory, yields only poor agreement in the vicinity of the excitation threshold, especially in the case of the $\underline{1s1s}$ double-excitation spectra. Furthermore, this satellite shows a quite large energy range to reach its saturation intensity. In the case of the $\underline{1s2p}$ emission a significantly smaller saturation range has been found, indicating a clear dependence of the intensity evolution on the shake shell.

Most recently, Galambosi *et al.* [19] continued the work of Deutsch *et al.* [15] by a study of the intensity evolution of the Cu $\underline{1s3d}$ satellites accompanying the Cu $K\alpha_{1,2}$ fluorescence from threshold to the saturation limit. They found a very short saturation range and were able to separate shake-up and shake-off thresholds taking into account the resonant Raman effect. They obtain a strong shake-up contribution R_u of 49% of the total shake probability at the saturation limit for these outer-shell electrons, which is in contrast to the results of the Ge $\underline{1s3p}$ and $\underline{1s3d}$ satellite intensity evolutions measured by Sternemann *et al.* [20] showing dominating shake-off behavior. In contrast to the results for the $\underline{1s2p}$ and $\underline{1s1s}$ satellite spectra, the intensity evolution of the $\underline{1s3d}$ Cu $K\alpha_{1,2}$ satellites could be well reproduced utilizing the Thomas model, thus validating the trend of increase in the saturation range with decreasing shell number of the shake electron. Until now, to our knowledge there exists no study of the dependence of the saturation range on the principal quantum number of the reemission electron filling the $\underline{1s}$ core hole.

Within this work we present measurements of the Cu $K\beta_{1,3}$ and Cu $K\beta_{2,5}$ x-ray emission spectra as a function of excitation energy in order to estimate the saturation behavior of the $\underline{1s3d}$ satellite contribution when different reemission processes are considered—namely, filling of the $\underline{1s}$ core hole
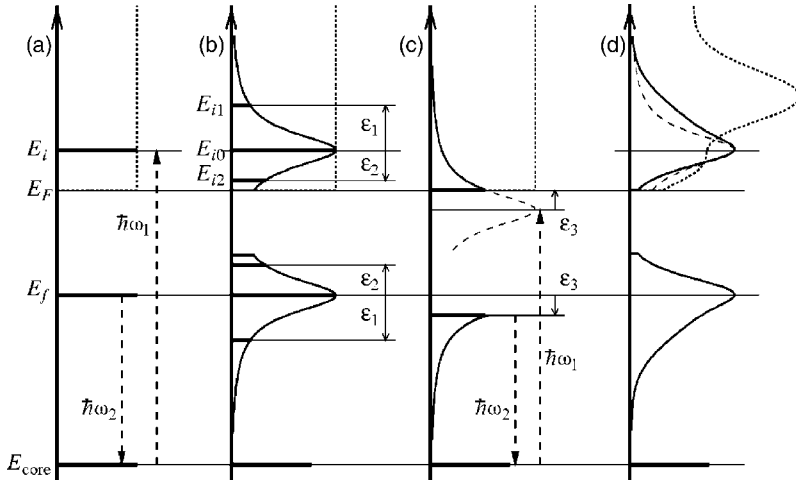
FIG. 1. Schematic visualization of the resonant Raman effect. Panels (a), (b), (c), and (d) are discussed in detail within the text.

by a $3p$ or $4p$ electron, respectively. The x-ray emission lines are fitted considering the diagram and satellite lines and the radiative Auger satellites as well as the resonant Raman effect. Within Sec. II the different contributions influencing the line shape of the x-ray emission spectra are disussed on a theoretical basis followed by a short description of the experiment in Sec. III. The experimental results are discussed in Sec. IV, whereas in Sec. V a short conclusion is given.

II. CALCULATION

If excited high above the absorption threshold, fluorescence lines can nicely be reproduced by assigning Lorentzians to each diagram and satellite line [15]. Then the width of each Lorentzian has to account for the natural width of the underlying multiplet as well as for the energetic broadening due to the finite lifetime of the intermediate and final states. This treatment is no longer valid if the excitation energy is in the vicinity of an absorption edge. The interplay of the core Lorentzian with the unoccupied density of states (u-DOS) causes a suppression of the high-energy tails of the fluorescence lines—i.e., the so-called resonant Raman effect [24,25]. The fluorescence spectrum I_{fluo} can be described via

$$I_{\text{fluo}}(\hbar\omega_2) \propto \int dE_i I^{\text{u}}(E_i) L(E_i - E_{\text{core}} - \hbar\omega_1)$$

$$\times \int dE_f I^{\text{o}}(E_f) \delta(E_i - E_f - \hbar\omega_1 + \hbar\omega_2), \quad (1)$$

where $I^{\text{u}}(E_i)$ and $I^{\text{o}}(E_f)$ symbolize the unoccupied and occupied densities of states (o-DOS), respectively, each multiplied by the corresponding transition matrix element to the core state E_{core}. The $\delta(E_i - E_f - \hbar\omega_1 + \hbar\omega_2)$ ensures the energy conservation of the total process, while $L(E_i - E_{\text{core}} - \hbar\omega_1)$ denotes the core Lorentzian

$$L(\epsilon) = \frac{1}{\epsilon^2 + (\Gamma/2)^2}, \quad (2)$$

characterized by the inverse lifetime of the core hole Γ and accounting for the energy conservation during absorption. The consequences of Eq. (1) are illustrated in Fig. 1. A con-

stant u-DOS (dotted line, E_{F} denotes the Fermi energy) and an o-DOS consisting of one single state at E_f are assumed in panels (a), (b), and (c). If the width of the core Lorentzian is equal to zero, only one unoccupied state with $E_i = E_{\text{core}} + \hbar\omega_1$ is accessible to the excited electron and the emission spectrum consists of one sharp line with $\hbar\omega_2 = \hbar\omega_1 - (E_i - E_f)$ [panel (a)]. If the core Lorentzian has a finite width, many unoccupied states E_i are accessible, each with a probability equal to the corresponding value of the Lorentzian $L(\epsilon)$ [panel (b)]. Thus, the single state E_f gives rise to a fluorescence spectrum with Lorentzian or at least truncated Lorentzian shape. If $E_{\text{core}} + \hbar\omega_1$ is close to or even below E_{F} [panel (c)], only part of the Lorentzian is covering the u-DOS, leading to the strongly asymmetric line shape typical for the resonant Raman effect. Moreover, the fine structure of the u-DOS has to be accounted for. For this purpose a more compact form of Eq. (1) can be obtained if E_{core} is defined to be zero and the intergal over E_f is performed. Finally the absorption intensity $I_{\text{abs}}(\epsilon)$ is defined to be the product of the core Lorentzian with the u-DOS ending up with

$$I_{\text{fluo}}(\hbar\omega_2) = \int d\epsilon I_{\text{abs}}(\epsilon) I^{\text{o}}(\hbar\omega_2 - \epsilon). \quad (3)$$

Thus the multiplet of occupied states has to be convoluted with the absorption intensity [see panel (d); the dashed line shows the truncated core Lorentzian, the dotted line the u-DOS, and the solid line the core Lorentzian after convolution]. This treatment is especially important in the case of the K edge of Cu where the u-DOS reaches its maximum only 13 eV above the absorption edge and thus deviations from a pure Lorentzian shape have to be expected even if $\hbar\omega_1$ exceeds the absorption edge by more than the energy width Γ.

Another contribution to the line shape of fluorescence lines is the radiative Auger satellites (RAS's). These occur if the electron system is shaken, by the electron which fills the inner-shell vacancy. Thus RAS's show no threshold behavior unlike the shake-up and shake-off excitations, where the electron system is shaken by the electron which is excited. In a radiative Auger process the energy set free during the relaxation of an electron into the inner-shell vacancy is only partly transferred to the Auger electron, while the rest of the

energy is emitted as a photon. From another point of view a fluorescence photon suffers an energy loss due to the simultaneous excitation of another electron into the unoccupied states. Therefore the resulting satellite feature is always situated on the low-energy side of the corresponding diagram line. The fraction of energy emitted as a photon can vary between zero and the Auger energy of the nonradiative process, giving rise to a broad feature extending over hundreds of electron volts with a slow decrease on the low-energy tail and with a steep drop towards the diagram line. The shape of these satellites can be described by

$$I_{\text{RAS}}(E) = I e^{d(E-E_0)}[1/(e^{(E-E_0)/w} + 1)], \qquad (4)$$

where the exponential characterized by the decay factor d accounts for the low-energy tail and the Fermi function creates the drop of the high-energy side. E_0 characterizes the onset energy and w the width of the drop.

Usually the integrated intensity of a RAS is only a few percent of its mother line [27] but in the case of valence fluorescence spectra of some late $3d$ elements (e.g., Co, Ni, Cu, Zn) it is a prominent feature, and a RAS is visible also in the $K\beta_{1,3}$ spectrum of Cu [31]. For these satellites the Auger electron is originating from the valence band where only a few eV are needed to excite the electron into the unoccupied states. Thus the RAS is overlapping the low-energy tail of the diagram line. The nomenclature for the radiative Auger satellites is identical to the nomenclature for the Auger lines. The first letter labels the principal quantum number of the inner-shell vacancies, the second labels the shell from which vacancy is refilled, and the third denotes the shell from where the Auger electron is excited. The radiative Auger satellites that are of interest in this work are the *KMN* and *KNN* satellites to the Cu $K\beta_{1,3}$ and $K\beta_{2,5}$ fluorescence lines, respectively.

III. EXPERIMENT

The measurements of the Cu $K\beta_{1,3}$ x-ray emission spectra were carried out at the bending magnet beamline G3 of HA-SYLAB (Hamburger Synchrotronstrahlungslabor, Hamburg, Germany). The incident radiation was monochromatized by a Ge 311 double-crystal monochromator and the fluorescence radiation was analyzed by means of a Rowland-type single-crystal spectrometer [31,32] with a Si 553 analyzer crystal on a Rowland circle of 1 m diameter in horizontal scattering geometry. The spectrometer is equipped with a position-sensitive gas proportional counter (PSD) having a spatial resolution of about 100 μm. A single fluorescence spectrum is obtained by combination of several PSD spectra taken at different positionings of the spectrometer. Thus the energy resolution of the spectrometer is not limited by the horizontal illumination of the sample by the incident photon beam. The scattering angle has been set to 90° to reduce Thomson scattering. Spectra of the fluorescence line of a polycrystalline Cu sample have been taken at several incident photon energies ranging from the Cu $1s$ binding energy of 8979 eV up to 9130 eV with an overall energy resolution of about 1 eV. The intensity of the incident radiation has been monitored using a NaI detector and an ionization chamber to guarantee
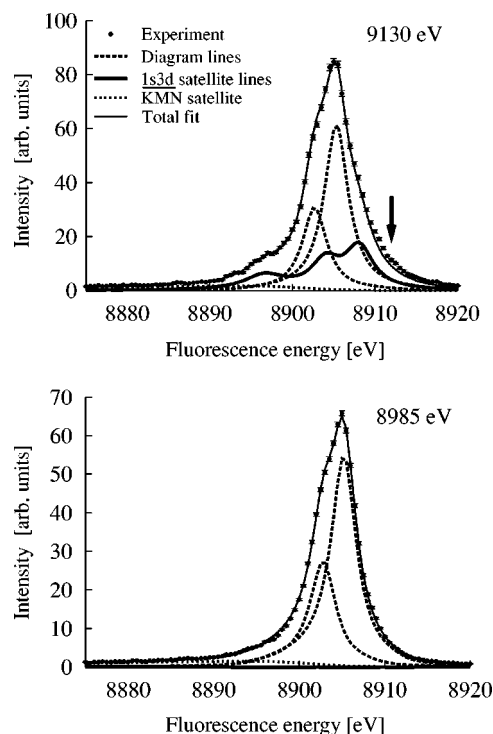

FIG. 2. X-ray emission spectra of the Cu $K\beta_{1,3}$ fluorescence line for two different excitation energies $\hbar\omega_1 = 8985$ eV and 9130 eV. The experimental data are shown as dots with error bars and are compared with the total fit function (thin solid line). The single contributions to the total excitation spectrum are presented in addition—namely, the diagram lines (dashed lines), the $\underline{1s3d}$ shake satellites (thick solid line), and the *KMN* radiative Auger satellite (dotted line). The arrow indicates the contribution from $\underline{1s3p}$ double ionization.

proper normalization of the fluorescence spectra.

The measurements of the Cu $K\beta_{2,5}$ valence fluorescence lines have been carried out at the beamline SAW2 (BL 9) of DELTA (Dortmund Electron Accelerator, Dortmund, Germany) [33]. The radiation supplied by the superconducting asymmetric wiggler was monochromatized using a Si 311 double-crystal monochromator and focused horizontally by means of a sagittally bend second monochromator crystal. The fluorescence radiation has been analyzed in horizontal scattering geometry at 90° scattering angle using the same Rowland spectrometer setup as discussed above. X-ray valence emission spectra have been measured for incident energies of 8995, 9005, 9020, 9050, and 9100 eV with an overall energy resolution of 2.2 eV. An ionization chamber and a NaI detector have been used for monitoring the incoming radiation. The experimental setup is described in more detail elsewhere [31].

IV. RESULTS AND DISCUSSION

The measured Cu $K\beta_{1,3}$ and Cu $K\beta_{2,5}$ x-ray emission spectra are shown for two excitation energies, one close to and the other far from the $1s$ binding energy, as dots with the corresponding error bar indicating the standard uncertainty in Figs. 2 and 3, respectively. The change in shape of both
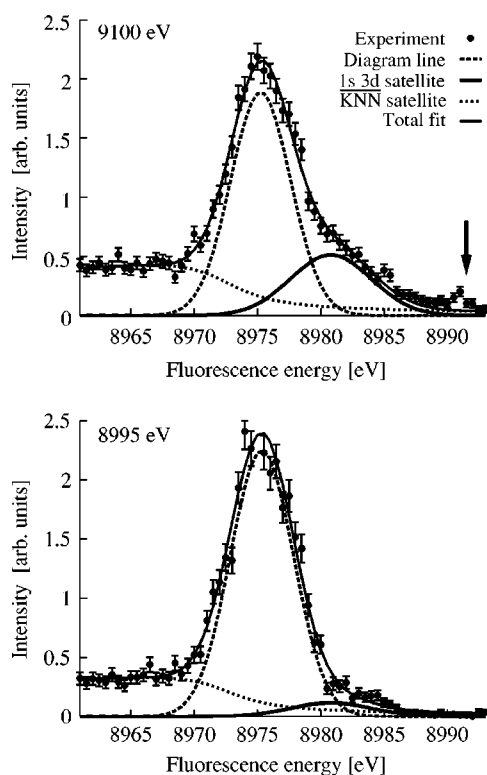
FIG. 3. X-ray emission spectra of the Cu $K\beta_{2,5}$ fluorescence line for two different excitation energies $\hbar\omega_1 = 8995$ eV and 9100 eV. The experimental data are shown as dots with error bars and are compared with the total fit function (thin solid line). The single contributions to the total excitation spectrum are presented in addition—namely, the diagram line (dashed line), the $\underline{1s3d}$ shake satellite (thick solid line), and the *KNN* radiative Auger satellite (dotted line). The arrow indicates the contribution from $\underline{1s3p}$ double ionization.

emission spectra is apparent and can be traced back to the appearance of the $\underline{1s3d}$ shake processes which will be discussed as follows.

The Cu $K\beta_{1,3}$ emission spectrum consists of the two diagram lines (dashed lines in Fig. 2) and the $\underline{1s3d}$ double excitation satellite spectrum (thick solid line) with its well-pronounced three-peak structure as discussed earlier by Deutsch *et al.* [15] with respect to their Dirac-Fock calculations. In addition a contribution from the *KMN* radiative Auger satellite (dotted line) is responsible for the low-energy tail of the fluorescence spectrum [31]. To separate and to quantify the different contributions to the emission spectrum, the experimental data are fitted assuming Lorentzians with identical widths and a height ratio of $I_{K\beta_3}/I_{K\beta_1} = 0.51$ for the diagram lines [15]. The satellite spectrum is modeled by three Lorentzians having fixed energy positions, widths, and relative intensities so that only the intensity of the total three-peak structure was varied during the fit procedure. Beforehand, the positions of the left and right peaks of this structure have been optimized by separate fits while the position of the center peak (8904 eV) has been taken from Ref. [15]. To account for the resonant Raman effect a measured Cu K absorption spectrum is deconvoluted from the core Lorentzian with $\Gamma = 1.55$ eV. For each $\hbar\omega_1$ this spectrum is multiplied

by the corresponding core Lorentzian again, yielding the absorption intensity $I_{abs}(\epsilon)$. Then the five Lorentzians describing the diagram and satellite lines are convoluted with $I_{abs}(\epsilon)$. However, this procedure yields good agreement between the fit function and the experimental data only for fluorescence energies $\hbar\omega_2 > 8890$ eV. The residual intensity at $\hbar\omega_2 < 8890$ eV is apparently due to the *KMN* radiative Auger satellite. Its line shape is modeled according to Eq. (4) where the onset energy $E_0 = 8900.8$ eV is given by the difference between the $K\beta_{1,3}$ fluorescence energy and the $3d$ binding energy in Cu, $w = 2.6$ eV is the half width at half maximum of the Cu $K\beta_{1,3}$ line, and the decay parameter d is fitted to be 0.023. Moreover, in the fluorescence spectrum excited at 9130 eV a residuum at 8912 eV (marked by the arrow) is visible but not considered within the fit procedure. This feature may be attributed to a $\underline{1s3p}$ shake satellite when compared to the relativistic Dirac-Fock calculations of Deutsch *et al.* [15].

The Cu $K\beta_{2,5}$ valence emission spectrum consists of one diagram line. Its high-energy tail shows a contribution originating from a $\underline{1s3d}$ double-ionization process. This diagram line and its $\underline{1s3d}$ satellite are modeled using pure Gaussians. A more sophisticated treatment is not appropriate due to the low signal-to-noise ratio of the available data set and due to the lack of adequate calculations. Furthermore, a strong contribution to the spectrum is given by the *KNN* radiative Auger satellite which is fitted by the same function as discussed above with $E_0 = 8973.3$ eV, $w = 3.0$ eV, and $d = 0.02$. In addition to the $\underline{1s3d}$ satellite a second excitation appeared at an excitation energy of 9100 eV at a fluorescence energy of 8991.5 eV marked by the arrow in Fig. 3. This feature has a width of 6 eV and may be related to a $1s3p$ double excitation, since the Zn $3p$ binding energy is $\overline{E_T(3p)} = 91.4$ eV, so that an excitation threshold of $E_T(\underline{1s3p}) = \overline{9070.3}$ eV is expected. Furthermore, the energy position of this feature is shifted by 16.5 eV to higher energies compared to the diagram line. This is close to the value of 14.1 eV obtained by the $Z+1$ approximation using $E_T(3p) = 91.4$ eV of Zn and $E_T(\underline{3p}) = 77.3$ eV of Cu.

Good overall agreement between the fits and experimental data of the Cu $K\beta_{1,3}$ as well as of the Cu $K\beta_{2,5}$ x-ray emission line is obtained. The intensities of the satellites show a distinct energy dependence. The relative intensities of the x-ray satellites R calculated by the integrated satellite intensity devided by the total fluorescence intensity are presented in Fig. 4. This total fluorescence intensity does not include the RAS contribution. The error bars are obtained by varying those parameters of the fit function that have been fixed during the fit—e.g., the positions, widths, and relative intensities of the three peaks of the Cu $K\beta_{1,3}$ satellite spectrum. These parameters are changed such that the fit residual does not exceed the 3σ error channel, yielding a spread of R for each excitation energy, being a measure for the error of R.

The $\underline{1s3d}$ satellite contribution of the Cu $K\beta_{1,3}$ emission spectrum shown in Fig. 4(a) increases rapidly and reaches its saturation intensity $R_\infty = 0.30$ very close to its excitation threshold. The spectra taken at excitation energies of 8985 eV, 8980 eV, and 8979 eV exhibit no significant satellite contribution within the limits of the experiment. At an
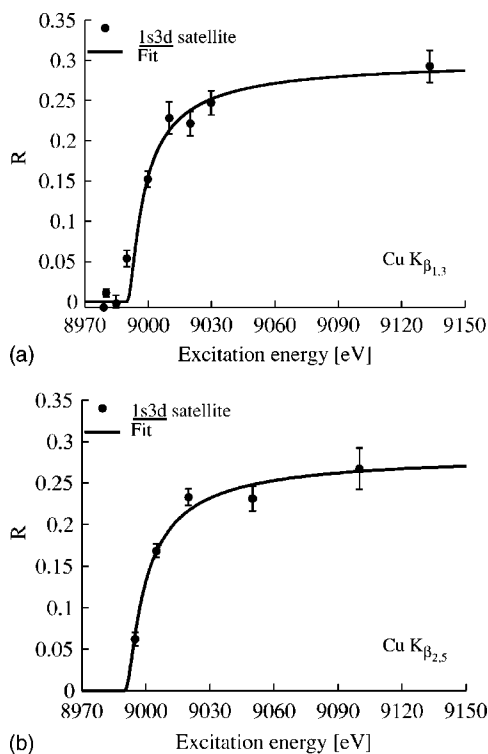
FIG. 4. (a) Intensity evolution of the Cu $K\beta_{1,3}\underline{1s3d}$ satellite contribution (dots with error bars) as a function of excitation energy compared to the best fit of the Thomas model to the experimental data as described within the text. The fit parameters are given in Table I. (b) Same as (a) but for the Cu $K\beta_{2,5}$ satellite contribution.

excitation energy of 8990 eV the satellite appears which gives a threshold energy of 8987.5 ± 2.5 eV. This is in line with the threshold energy $E_T(\underline{1s3d})=8989.1$ eV estimated using the $Z+1$ approximation by assuming the $1s$ binding energy to $E_T(\underline{1s})=8978.9$ eV and the $3d$ electron binding energy of Zn $E_T(\underline{3d})=10.2$ eV [34]. The intensity evolution indicates mainly shake-off character of the excitation. The upper limit for a possible shake-up contribution is given by $R_u=0.054\pm0.01$ according to the error bar of R for the excitation energy of 8990 eV which is significantly smaller compared to the shake-up probability of $R_u=0.13$ obtained for the Cu $K\alpha_{1,2}$ emission spectrum by Galambosi *et al.* [19], whereas the saturation intensities are in good agreement.

The $\underline{1s3d}$ satellite contribution of the Cu $K\beta_{2,5}$ emission spectrum presented in Fig. 4(b) behaves similar compared to the Cu $K\beta_{1,3}$ spectra with respect to the excitation threshold

and its saturation behavior. The saturation intensity is estimated to $R_\infty\approx0.29$. Measurements for excitation energies smaller than 8995 eV were not performed, so that the threshold energy could not be determined in this case properly.

The intensity evolution of the $\underline{1s3d}$ satellites is fitted to the Thomas model [30], which describes the saturation behavior of shake-off double-excitation intensities R from the adiabatic to the isothermal regime within a simple mathematical form by

$$R = R_\infty e^{[-r_s^2 E_s^2/15.32(E-E_T)]},$$

where R_∞ is the saturation limit, r_s the radius of the $3d$ shake shell, and $E_s=E_T(\underline{1s3d})-E_T(\underline{1s})$ the shake energy which has been determined using the $Z+1$ model to be 10.2 eV. E and E_T are the excitation and threshold energy, and the excess energy is defined via $E_{ex}=E-E_T$. The adjustable parameters are R_∞ and r_s, whereas E_T was fixed to the value of $E_T(\underline{1s3d})=8989.1$ eV. The results of the fits are plotted as solid line in Figs. 4(a) and 4(b). The Thomas model reproduces well the intensity evolution of both satellite spectra with its very short saturation range. All parameters for the fit are given in Table I. The results obtained for the shake shell radius of 1.03 Å and 1.12 Å for the Cu $K\beta_{1,3}$ and Cu $K\beta_{2,5}$ fluorescene, respectively, are close to the average $3d$ shell radius of 0.85 Å given by a relativistic multiconfigurational Dirac-Fock calculation [19]. The fit parameters in this work are also in good agreement with the results obtained for the Cu $K\alpha_{1,2}$ emission spectrum of Ref. [19].

The experimental data of the satellite intensity as a function of excess energy E_{ex} along with the corresponding fits to the Thomas model of this work are compared to the results of the Thomas fit for the different Cu $K\alpha_{1,2}$ satellites— namely, $\underline{1s3d}$ of Ref. [19], $\underline{1s2p}$ of Ref. [17], and $\underline{1s1s}$ of Ref. [18]—in Fig. 5. The relative satellite intensities have been normalized to their corresponding saturation intensities. The fit parameters are shown in Table I. The measurements of the Cu $K\beta_{1,3}$ and Cu $K\beta_{2,5}$ $\underline{1s3d}$ satellite spectra confirm the strong dependence of the saturation behavior of the satellite intensities on the principal quantum number of the shake electron. The saturation range decreases rapidly with increasing quantum number. Furthermore, the saturation behavior is unaffected by the reemission process when the shake shell is kept constant but the shell of the electron filling the $1s$ core hole is changed. These results may give the possibility to decouple excitation and deexcitation processes in the theoretical treatment of multi-ionization processes.

TABLE I. Summary of the fit parameters used for the Thomas model in Refs. [17–19] and this work. E_T denotes the threshold energy, E_s the shake energy, r_s the radius of the shake shell, and R_∞ the saturation intensity of the double-excitation satellites. In Ref. [18] no value for R_∞ is given.

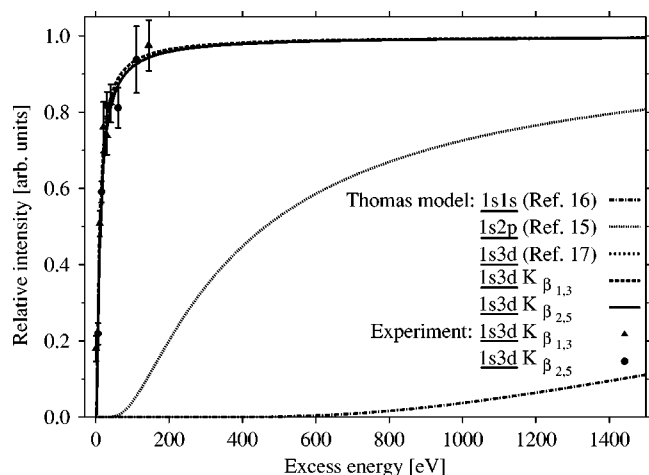| Excitation	Emission	E_T [eV]	E_s [eV]	r_s [Å]	R_∞
$1s1s$ (Ref. [18])	$K\alpha_{1,2}$	17372.0	9366.3	0.024	—
$1s2p$ (Ref. [17])	$K\alpha_{1,2}$	9922.0	1002.0	0.07	0.88
$1s3d$ (Ref. [19])	$K\alpha_{1,2}$	8989.1	10.2	1.10	0.265
$1s3d$ (this work)	$K\beta_{1,3}$	8989.1	10.2	1.03	0.30
$1s3d$ (this work)	$K\beta_{2,5}$	8989.1	10.2	1.12	0.29

FIG. 5. Intensity evolution of the Cu $K\beta_{1,3}$ (dots with error bars) and the Cu $K\beta_{2,5}$ (triangles with error bars) $\underline{1s3d}$ satellite contribution as a function of excess energy presented with the corresponding fits to the Thomas model (long dashed and solid lines). The results of this work are compared to Thomas fits of the $\underline{1s3d}$ (dotted line) [19], $\underline{1s2p}$ (short dashed line) [17], and $\underline{1s1s}$ (dash-dotted line) [18] emission spectrum. The corresponding fit parameters are given in Table I.

The consideration of the RAS turned out to be indispensible in the interpretation of the x-ray emission spectra. The peak intensities of the RAS normalized to the intensities of its diagram lines show no significant dependence on the excitation energy above threshold. Especially in the case of the *KMN* satellite the normalized intensities are constant in the measured energy range. The peak intensity of the *KNN* satellite of the Cu $K\beta_{2,5}$ emission spectrum increases slowly with increasing excitation energy, which may be due to contributions of $\underline{1s3d}$ excitation channels underlying the diagram line which cannot be separated properly. Since fluorescence energies have been measured only close to the diagram lines, it is not possible to determine the integrated intensities for the RAS. However, the significantly strong contribution of the *KNN* satellite to the valence emission spectrum compared to the *KMN* contribution to the Cu $K\beta_{1,3}$ emission

lines is apparent and emphasizes the importance of considering RAS in the interpretation of valence fluorescence spectra.

V. CONCLUSION

In conclusion, this study presents an investigation of double-excitation processes at the Cu $K\beta_{1,3}$ and Cu $K\beta_{2,5}$ x-ray emission spectra. The energy dependence of the shape of the emission spectra was accurately modeled considering the corresponding diagram and $\underline{1s3d}$ satellite lines along with a contribution from radiative Auger processes. Furthermore, indications of additional satellites due to $\underline{1s3p}$ excitation have been found. The intensity evolution of $\underline{1s3d}$ satellites could be well explained utilizing the Thomas model. The experimental results of the Cu $K\beta_{1,3}$ emission spectrum indicate an upper limit for shake-up contributions to the total shake intensity of 20%. The results confirm the trend that the saturation range increases rapidly with decreasing shake shell number, and the double excitation was shown to be independent of the shell number of the reemission electron within the limits of the experiment. This behavior is not yet explained by any model and demands highly accurate calculations of these satellite intensities close to threshold. Furthermore, the *KMN* and *KNN* radiative Auger satellites contribute significantly to the fluorescence spectra and have to be considered in the inerpretation of fluorescence spectra.

[1] *Atomic Inner Shell Physics*, edited by B. Crasemann (Plenum, New York, 1986).

[2] G. B. Armen, T. Åberg, K. R. Karim, J. C. Levin, B. Crasemann, G. S. Brown, M. H. Chen, and G. E. Ice, Phys. Rev. Lett. **54** 182 (1985).

[3] T. Åberg, in *Conference on Inner-Shell Ionization Phenomena and Future Applications*, edited by R. W. Finkk, S. T. Manson, J. M. Palms, and P. Venugopala Rao, U.S. AEC Report No. CONF-720404 (National Technical Information Service, U.S. Dept. of Commerce, Springfield, VA, 1972), p. 1509.

[4] B. Crasemann, J. Phys. (Paris), Colloq. **48**, C9–3 (1987); Can. J. Phys. **76**, 251 (1989).

[5] M. Deutsch and M. Hart, Phys. Rev. Lett. **57**, 1566 (1986).

[6] G. Li, F. Bridges, and G. S. Brown, Phys. Rev. Lett. **68**, 1609

(1992).

[7] S. J. Schaphorst, A. F. Kodre, J. Ruscheinski, B. Crasemann, T. Åberg, J. Tulkki, M. H. Chen, Y. Azuma, and G. S. Brown, Phys. Rev. A **47**, 1953 (1993).

[8] J. Chaboy, A. Marcelli, and T. A. Tyson, Phys. Rev. B **49**, 11 652 (1994).

[9] A. Filipponi and A. Di Cicco, Phys. Rev. A **52**, 1072 (1995).

[10] J. Padežnink Gomilšek, A. Kodre, I. Arčon, and Rok Preseren, Phys. Rev. A **64**, 022508 (2001).

[11] K. Siegbahn, C. Nordling, G. Johansson, J. Hedman, P. F. Hedén, K. Harmin, U. Gelius, T. Bergmark, L. O. Werme, and Y. Bear, *ESCA Applied to Free Molecules* (North-Holland, Amsterdam, 1969).

[12] D. L. Wark, R. Bartlett, T. J. Bowles, R. G. H. Robertson, D. S.

Sivia, W. Trela, J. F. Wilkerson, G. S. Brown, B. Crasemann, S. L. Sorensen, S. J. Schaphorst, D. A. Knapp, J. Henderson, J. Tulkki, and T. Åberg, Phys. Rev. Lett. **67**, 2291 (1991).

[13] T. Mukoyama and Y. Ito, Nucl. Instrum. Methods Phys. Res. B **87**, 26 (1994).

[14] R. D. Deslattes, R. E. La Villa, P. L. Cowan, and A. Henins, Phys. Rev. A **27**, 923 (1983).

[15] M. Deutsch, G. Hölzer, J. Härtwig, J. Wolf, M. Fritsch, and E. Förster, Phys. Rev. A **51**, 283 (1995).

[16] M. Deutsch, O. Gang, K. Hämäläinen, and C. C. Kao, Phys. Rev. Lett. **76**, 2424 (1996).

[17] M. Fritsch, C. C. Kao, K. Hämäläinen, O. Gang, E. Förster, and M. Deutsch, Phys. Rev. A **57**, 1686 (1998).

[18] R. Diamant, S. Huotari, K. Hämäläinen, C. C. Kao, and M. Deutsch, Phys. Rev. Lett. **84**, 3278 (2000); R. Diamant, S. Huotari, K. Hämäläinen, C. C. Kao, and M. Deutsch, Phys. Rev. A **62**, 052519 (2000).

[19] S. Galambosi, H. Sutinen, A. Mattila, K. Hämäläinen, R. Sharon, C. C. Kao, and M. Deutsch, Phys. Rev. A **67**, 022510 (2003).

[20] C. Sternemann, A. Kaprolat, M. H. Krisch, and W. Schülke, Phys. Rev. A **61**, 020501 (2000).

[21] R. Diamant, S. Huotari, K. Hämäläinen, R. Sharon, C. C. Kao, and M. Deutsch, Phys. Rev. A **63**, 022508 (2001).

[22] P.-A. Raboud, M. Berset, J.-Cl. Dousse, Y.-P. Maillard, O. Mauron, J. Hoszowska, M. Polasik, and J. Rzadkiewicz, Phys. Rev. A **65**, 062503 (2002).

[23] M. Oura, T. Mukoyama, M. Taguchi, T. Takeuchi, T. Haruna, and S. Shin, Phys. Rev. Lett. **90**, 173002 (2003).

[24] P. Eisenberger, P. M. Platzman, and H. Winick, Phys. Rev. B **13** 2377 (1976).

[25] K. Hämäläinen, S. Manninen, P. Suortti, S. P. Collins, M. J. Cooper, and D. Laundry, J. Phys.: Condens. Matter **1** 5955 (1989).

[26] T. Åberg, Phys. Rev. A **4**, 1735 (1971).

[27] O. Keski-Rahkonen and J. Ahopelto, J. Phys. C **13**, 471 (1980).

[28] Yeon Deog Koo and K. Das Gupta, Phys. Rev. A **42**, 5441 (1990).

[29] Ch. Herren and J.-Cl. Dousse, Phys. Rev. A **56**, 2750 (1997).

[30] T. D. Thomas, Phys. Rev. Lett. **52**, 417 (1984).

[31] H. Enkisch, Ph.D. thesis, University of Dortmund, Dortmund, Germany, 2001.

[32] W. Schülke, A. Kaprolat, Th. Fischer, K. Höppner, and F. Wohlert, Rev. Sci. Instrum. **66**, 2446 (1995).

[33] Dortmund Electron Accelerator (DELTA), University of Dortmund, Maria-Goeppert-Mayer-Str. 2, D-44221 Dortmund, Germany (www.delta.uni-dortmund.de).

[34] The Zn and Cu 3d and 3p electron binding energies have been taken from A. C. Thompson *et al.*, Report No. LBNL/PUB-490 Rev 2, 2001 (unpublished).